International Journal of Heat and Technology
Vol. 42, No. 6, December, 2024, pp. 2058-2066
Journal homepage: http://iieta.org/journals/ijht

Alternative Use of MJ2955 Transistor as a Substitute for Solar Panels in Simple Power Plants

Rombe Allo[1], Selyus Rantepulung[1], Allo Sarira Pongsapan[1], Samuel P. Siregar[1], Enos Tambing[1], Oktavianus Kati[2], Joni[3*]

[1] Department of Mechanical Engineering, Cenderawasih University, Papua 99351, Indonesia
[2] Department of Electrical Engineering, Cenderawasih University, Papua 99351, Indonesia
[3] Master Program in Renewable Energy Engineering, Postgraduate Program, Cenderawasih University, Papua 99351, Indonesia

Corresponding Author Email: joni@ftuncen.ac.id

https://doi.org/10.18280/ijht.420623

Received: 8 October 2024
Revised: 24 November 2024
Accepted: 7 December 2024
Available online: 31 December 2024

Keywords:
electrical power, panel efficiency, energy conversion, MJ2955 transistor solar panel, DC voltage

ABSTRACT

This study examines the application of the MJ2955 transistor as a replacement for photovoltaic panels in simple power plants to facilitate low-cost electricity supply. The panels are constructed from plywood sheets measuring 30 cm × 40 cm × 0.3 cm. A total of 35 transistors are used; the entire top cover of each MJ2955 transistor is removed, after which they are arranged on a board, pasted, and connected with 0.35 mm nickel wire. The investigation, conducted over a singular day from 9:00 AM to 3:00 PM, sought to gather information regarding the electric current and voltage generated by solar irradiation in the transistor circuit. Results from the trials indicated a maximum voltage of 15.33 Volts at 11:00 AM, and an electric current consistently measured at 0.04 mA between noon and 02:00 PM. The output power peaked at 0.00063 Watts, with a maximum efficiency of 1.313%. This indicates the potential of transistors for applications involving solar cell replacement, although certain constraints, such as voltage fluctuations and resistance, affect output stability. Resistance decreases at high intensity, thus increasing output power. The study shows that the MJ2955 transistor has potential as an alternative for low-power solar applications used for electric lighting in remote communities.

1. INTRODUCTION

The global demand for renewable energy solutions continues to grow exponentially, driven by environmental concerns and the urgent need for sustainable power generation methods [1, 2]. Although solar photovoltaic technology persists as the preeminent resolution in sustainable energy, its application encounters numerous obstacles, encompassing elevated initial expenditures, climatic reliance, and upkeep necessities [3]. These obstacles have prompted investigations into alternative power generation methods, particularly in regions lacking access to traditional renewable energy technologies. Exploring semiconductor devices for power generation is a new field worthy of further investigation [4]. The MJ2955 transistor, traditionally used as a power transistor in amplification circuits, has shown unexpected potential in direct power generation applications. These PNP silicon transistors, known for their robust construction and reliable performance in high-power applications, exhibit unique characteristics under certain environmental conditions [5]. Previous research has shown that semiconductor junctions can generate small electrical potentials under specific thermal and electromagnetic conditions [6], However, the systematic application of this principle using common transistors is still largely unexplored.

Recent advances in semiconductor physics have revealed that transistors can function outside of their conventional roles when subjected to controlled environmental stimuli [7]. The unique PN junction configuration and the relatively large surface area of the MJ2955 make it an attractive candidate for alternative power generation research. Initial observations suggest that these transistors, if properly configured, can generate a measurable electrical potential without an external power input, potentially offering a cost-effective alternative to traditional solar cells for specific applications [8].

Understanding these aspects is essential for developing practical applications, especially in areas where traditional solar panels face significant obstacles. This research builds on foundational work in semiconductor physics while exploring new applications that could revolutionize small-scale power generation approaches [9].

This investigation holds significant relevance in light of the current global emphasis on advancing a diverse range of renewable energy solutions. Although the power output from transistor-based generators may not match that of conventional solar panels on a large scale, its potential applications in low-power electronics and sensor systems warrant comprehensive investigation [10]. The simplicity and accessibility of the MJ2955 transistor, combined with its rugged construction and wide availability, make it an intriguing subject for alternative power generation research.

This research aims to explore the use of the MJ2955 transistor as a substitute for solar cells in the development of small-scale power generation systems and potentially open new avenues for power plant research.

2. LITERATURE REVIEWS

The topography of solar energy transmutation has undergone a noteworthy metamorphosis in contemporary years, characterized by substantial technological advancements and augmented efficiency across diverse platforms. In silicon-based photovoltaic technology, Kobayashi et al. [11] reported unprecedented achievements with N-type TOPCon cells reaching an efficiency of 26.8%, while heterojunction cells (HJT) demonstrated an efficiency of 25.7% under laboratory conditions. This advancement is complemented by innovative work [12] on surface textures, which achieves a 15 % increase in light absorption through the diamond-shaped micro-texture technique, fundamentally reducing reflection loss to below 2%. Perovskite photovoltaic cells have surfaced as an exceptionally auspicious domain, with chronicling a remarkable efficacy advancement of 25.9% for singular-junction cells and 31.3% for tandem silicon-perovskite assemblies [8, 13]. Despite critical stability challenges, new encapsulation techniques have been developed that extend operational life by up to 300% and improve moisture resistance with advanced hydrophobic coatings, maintaining stability at temperatures up to 85°C for more than 2000 hours [14, 15].

Multi-junction photovoltaic cells have demonstrated remarkable capability for elevated-efficiency applications, as substantiated by the research of Jung et al. [6]. Achieving a notable efficiency of 39.2%, the triple-junction cell stands out, while the quadruple-junction architecture impressively reaches 43.1% efficiency under concentrated light. Polly et al. [16] further advanced this field by investigating the combination of new III-V semiconductors and improved tunnel junction designs, significantly enhancing spectral absorption while reducing production costs by up to 35%. These advancements not solely anticipate to transform energy transmutation but additionally facilitate the emergence of more sustainable production methodologies, congruent with worldwide initiatives to diminish the carbon footprint of the solar sector.

Concentrated Photovoltaic (CPV) systems are experiencing considerable progress in their operational efficacy and financial dependability. Zou et al. [17] illustrated a concentrated system that achieved a 44.5% efficacy, combined with a forward-thinking tracking solution that minimized energy expenditure by 40%. This system was also paired with a novel tracking mechanism that cut energy consumption by 40%. Mohamadi and Karbasian [18] documented a 45% reduction in production costs through improved optical systems and enhanced reliability measures, extending the system's life to more than 30 years.

Emerging technologies show promising advances, especially in quantum dot solar cells, where Zhou et al. [19] demonstrated an increase in efficiency of up to 18.1% with an extended spectral response into the near-infrared region. Significant advances in organic photovoltaics have also been made, achieving 19.2% efficiency while enhancing flexible substrate applications and roll-to-roll manufacturing capabilities [20]. Integration technology has advanced rapidly, developing an integrated battery system with 92% round-trip efficiency and advanced power electronics that reduce losses by 25%. Azimi el al. [21] have successfully advanced network consolidation, recording an inverter efficiency enhancement of as much as 99% and implementing sophisticated predictive algorithms that lessen throttling by up to 40%.

Innovation has assumed an essential role in propelling the commercialization of solar technology. He et al. [22] and Qu et al. [23] reported on an automated manufacturing line that reduces expenses by 35% while preserving enhanced quality control, resulting in a defect rate falling below 0.1%. Westerband and Hicks [24] contributed to considerable material enhancements, diminishing the use of silver by as much as 80% and prolonging the lifespan of products to over 35 years through refined encapsulation materials. Environmental impact assessments are becoming progressively vital, with Kuo et al. [25] recording a 45% diminution in the carbon footprint of production and a 60% abatement in water utilization.

A comprehensive life cycle assessment demonstrates a 0.5-year reduction in energy payback duration and an overall decrease in environmental impact of 35% [26, 27]. Furthermore, numerous critical research foci have been delineated, encompassing building-integrated photovoltaics, extraterrestrial solar, and hybrid energy frameworks [28]. Substantial research gaps persist in areas such as the long-term stability of novel materials, economical energy storage solutions, and advanced recycling technologies. The ongoing enhancement of solar energy conversion technologies suggests notable advancements in efficiency, cost benefits, and ecological sustainability, making solar energy a more viable solution to the energy challenges faced globally.

3. MATERIALS AND METHODS

The research examining the potential application of the MJ2955 transistor as a substitute for photovoltaic panels was conducted in the Laboratory of the Department of Mechanical Engineering at Cenderawasih University, located at the geographical coordinates 2°34'57"S, 140°38'55"E, as illustrated in Figure 1.

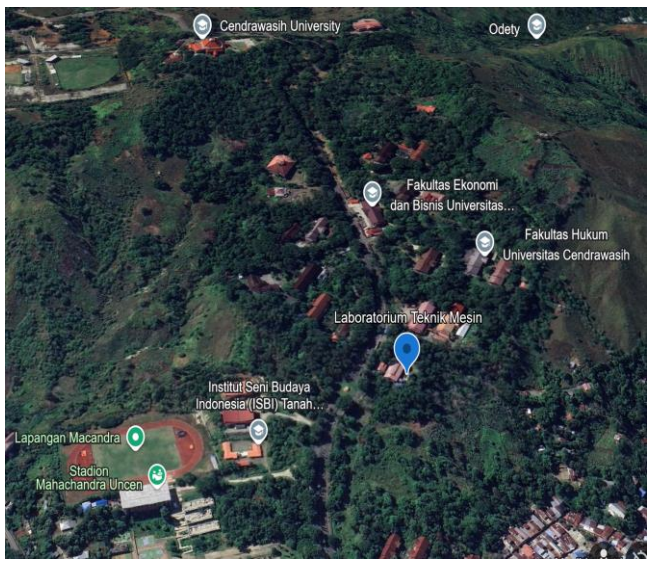

Figure 1. Coordinates of the test location

3.1 Panel preparation and fabrication

The MJ2955 transistor was selected for its ability to generate electrical power (Figure 2). The choice of the MJ2955 PNP transistor is based on its electrical characteristics, including current amplification, saturation voltage, and thermal resilience, all of which are crucial for effective energy conversion [29]. The circuit for the MJ2955 transistor is designed to convert solar energy into electrical energy.

Figure 2. MJ2955 transistor construction

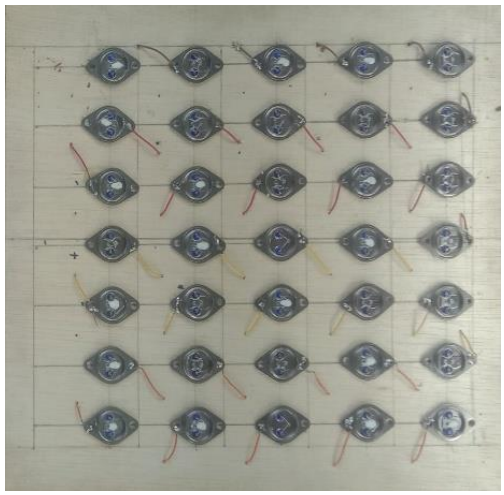

Figure 3. MJ2955 transistor panel prototype

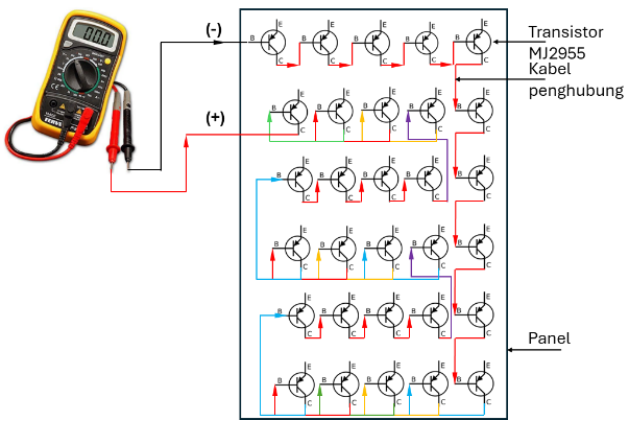

Figure 4. MJ2955 transistor panel circuit diagram

The MJ2955 transistor is attached to a plywood panel measuring 30 cm × 40 cm × 0.3 cm (Figure 3), which has been pre-drilled to accommodate the transistor terminals before being glued together. Each transistor terminal C is connected in series to the other transistor terminal B using a 0.35 mm nickel conductor, in accordance with the circuit illustrated in Figure 4, and is further secured with solder.

Before determining the number of transistors needed, a circuit panel must produce a DC mains voltage of ±15 Volts. It first evaluates the voltage and current for each transistor intended for use. The upper casing of the transistor is removed using a hacksaw. Each transistor is placed in direct sunlight to measure its voltage output and electrical current with a multimeter. When subjected to sunlight, the voltage and electrical current generated range from 0.38 to 0.5 Volts and 0.0006 to 0.0018 mA, respectively; thus, the aggregate number of transistors employed is 35 units to achieve an output voltage of 15 Volts.

3.2 Data collection

This study assesses the efficacy of an M2955 transistor-based panel installation with an anticipated electrical voltage output of ±12 Volts. The panels are positioned in an open testing environment specifically arranged to receive direct sunlight. Between 09:00 AM and 03:00 PM, data was collected, featuring 20-minute gaps for the gathering process. The input variables—light intensity, temperature, and relative humidity—are sourced from data supplied by the Global Solar Atlas and NASA Power Data [30]. The output variables, voltage and current, are measured using a multimeter.

3.3 Data analysis

The collected data consisted of measurement data (voltage and electric current) and solar potential data from the Global Solar Atlas, based on the coordinate points of the test site, which included direct normal irradiation, temperature, and relative humidity.

3.3.1 Statistical tests

The compiled data underwent scrutiny through descriptive statistical techniques, encompassing central tendency indicators including the mean and median, as well as variability indicators like range and standard deviation.

3.3.2 Panels efficiency

The energy transformation efficacy is computed by contrasting the incoming solar energy with the electrical yield, employing the subsequent equation [31]:

$$\eta = \frac{P_{output}}{P_{input}} \times 100\% \quad (1)$$

where, P_{output} is the power produced by the panel (Watts); and P_{input} is determined from solar radiation and the surface area of the transistor element exposed to sunlight (Watts).

Input power (P_{in}) is the power obtained from direct normal irradiation (DNI) absorbed by the surface area of the PNP transistor,

$$P_{input} = DNI \times A \quad (2)$$

where, DNI is direct normal irradiation (Wh/m^2); and A is the

surface area of the transistor PNP element (m^2).

The electrical output power generated by the panel is determined using the equation [32]:

$$P_{output} = V \times I \quad (3)$$

where, V is the measured voltage (Volts); and I is the electric current (Amps).

4. RESULTS AND DISCUSSION

4.1 Characteristics of solar irradiation

Solar irradiance is contingent upon spatial positioning and local circumstances, including moisture, atmospheric pressure, and velocity of wind. The test location for the MJ2955 transistor assembly, instead of the solar panel, is situated at the coordinates 2°34'57"S, 140°38'55"E. Utilizing the Global Solar Atlas, location-specific information is obtained (Table 1), including the average direct normal irradiation per hour (Wh/m²) and the solar path.

Table 1. Daily location information data

Parameter	Value	Unit
Direct normal irradiation	3.569	kWh/m²
Global horizontal irradiation	4.894	kWh/m²
Diffused horizontal irradiation	2.276	kWh/m²
Global tilt irradiation at optimal angle	4.910	kWh/m²
Temperatures	26.1	℃
Optimal PV module tilt	5	°
Terrain elevation	162	m

4.1.1 Direct normal irradiation (DNI)

Average DNI per hour, articulated in watt-hours per square meter (Wh/m²), constitutes a significant metric in solar energy applications. It quantifies the mean quantity of solar energy that impacts a surface perpendicular to solar radiation for a duration of one hour. DNI specifically considers solely the direct constituents of solar radiation, omitting diffuse radiation disseminated by the atmosphere. This direct solar energy possesses the highest energy potential and is pivotal for concentrated solar power technologies that utilize panels to harness solar radiation.

Figure 5 presents an exposition of the hourly distribution of DNI in Wh/m², evaluated over the course of the year. From 12:00 AM. to 06:00 PM and then from 06:00 PM to 12:00 AM, the DNI remained at zero, which means there was no direct radiation intensity noted at this time, seemingly because the sun was beneath the horizon. From 06:00 AM onwards, radiation levels escalate rapidly, signifying a phase of productive solar activity. The summit values reliably manifest between 10:00 PM and 02:00 PM, when the sun is at its pinnacle, achieving maximum radiation levels.

From May to October, the mean DNI value is superior in comparison to that of other months. May registered the highest aggregate (3994 Wh/m²), whereas January, February, November, and December exhibited lower totals, likely attributable to seasonal influences such as overcast weather or diminished solar angles during these months [33].

4.1.2 Solar trajectories

The horizon constitutes the demarcation between the terrestrial surface and the firmament as perceived from a designated vantage point, appearing as a horizontal plane that seemingly intersects the celestial sphere, thereby creating a circumference surrounding the observer. It functions as a reference datum for quantifying the angle of solar elevation, which denotes the altitude of the sun above the horizon [34]. Conversely, the trajectory of the sun pertains to the apparent course of the sun traversing the sky as observed from a specific location on Earth throughout the diurnal cycle and annually. The sun's trajectory is determined by several elements, such as the rotating Earth, its tilt of nearly 23.5 degrees, and the observer's latitude [35]. Consequently, the solar trajectory fluctuates with the seasonal changes and the geographical position of the observer.

Based on the examination of the solar trajectory diagram in Figure 6, this location resides within the WIT time zone (UTC+09:00). The solar movement can be monitored from 06:00 AM to 17:00 PM, exhibiting three principal trajectories that delineate the sun's position throughout the annual cycle. During the June solstice (shown in blue), the apex trajectory materializes, the equinox (shown in black) reveals the intermediate trajectory, and the nadir trajectory presents itself at the December solstice (shown in red).

The solar elevation angle is measured on the perpendicular axis from 0° at the horizon to 90° at the zenith, whereas the azimuth angle is measured horizontally from 0° to 360°, utilizing reference points at 45° intervals (0°, 45°, 90°, 135°, 180°, 225°, 270°, and 315°) [35].

Hours	Date																													
	1	2	3	4	5	6	7	8	9	10	11	12	13	14	15	16	17	18	19	20	21	22	23	24	25	26	27	28	29	30
0 - 1	0	0	0	0	0	0	0	0	0	0	0	0	0	0	0	0	0	0	0	0	0	0	0	0	0	0	0	0	0	0
1 - 2	0	0	0	0	0	0	0	0	0	0	0	0	0	0	0	0	0	0	0	0	0	0	0	0	0	0	0	0	0	0
2 - 3	0	0	0	0	0	0	0	0	0	0	0	0	0	0	0	0	0	0	0	0	0	0	0	0	0	0	0	0	0	0
3 - 4	0	0	0	0	0	0	0	0	0	0	0	0	0	0	0	0	0	0	0	0	0	0	0	0	0	0	0	0	0	0
4 - 5	0	0	0	0	0	0	0	0	0	0	0	0	0	0	0	0	0	0	0	0	0	0	0	0	0	0	0	0	0	0
5 - 6	37.22	42.91	10.60	12.12	29.68	15.40	31.76	19.01	25.31	52.03	27.37	27.28	29.58	34.44	0.00	0.00	0.00	0.00	0.00	0.00	0.00	0.00	0.00	0.00	0.00	0.00	0.00	0.00	0.00	0.00
6 - 7	275.41	411.20	61.40	40.17	418.34	73.91	380.05	90.91	262.72	352.47	34.05	57.05	28.79	185.08	59.77	239.40	70.16	48.74	44.24	29.63	288.30	206.27	476.90	63.80	50.08	289.23	27.96	156.28	36.39	31.02
7 - 8	488.95	633.21	74.08	131.21	658.23	276.59	648.05	347.53	547.08	632.25	64.42	198.84	35.75	471.21	214.02	482.66	116.73	58.70	156.28	29.88	477.85	276.45	679.25	129.11	103.33	644.36	43.29	286.27	83.07	36.08
8 - 9	696.57	736.88	108.93	157.72	848.82	408.52	760.05	518.64	649.27	719.86	99.66	269.27	47.30	530.90	344.96	598.62	192.45	92.27	297.16	30.42	**475.76**	391.19	806.54	81.52	152.20	766.14	50.95	425.59	156.47	48.59
9 - 10	575.16	557.34	144.33	154.10	809.77	380.63	717.44	707.30	610.83	711.53	185.04	356.30	59.57	566.73	541.24	538.12	204.79	127.48	121.35	35.04	**267.45**	365.24	769.48	102.23	235.78	679.28	82.84	490.49	120.92	65.42
10 - 11	738.52	669.34	124.79	161.39	859.76	400.73	789.01	727.14	661.99	687.77	246.80	275.42	80.16	457.19	640.97	519.02	197.46	179.29	57.05	67.57	**167.75**	301.36	796.66	133.28	335.44	749.43	142.62	603.59	125.20	67.11
11 - 12	682.34	596.13	114.82	251.67	885.97	402.10	721.53	713.01	693.04	583.34	291.59	186.61	94.05	418.69	701.41	392.66	182.19	217.77	127.31	126.45	**202.35**	287.14	678.27	125.00	399.48	681.26	222.97	526.48	150.83	89.70
12 - 13	571.28	606.72	55.70	494.91	802.45	356.94	678.44	668.06	667.38	506.20	253.38	177.08	91.56	416.29	692.60	304.42	176.18	244.08	140.62	91.61	**273.30**	306.59	563.62	150.09	436.56	706.59	207.33	533.29	175.09	75.65
13 - 14	502.45	547.81	40.24	547.45	885.79	365.46	565.15	490.84	658.30	508.00	263.02	133.05	97.42	475.04	623.05	378.45	133.27	203.33	110.15	80.16	**269.86**	308.77	517.53	174.79	357.18	648.27	160.15	615.59	217.86	55.40
14 - 15	546.20	541.93	51.80	684.31	771.53	333.80	544.85	313.23	656.95	419.49	230.05	85.65	77.01	627.66	537.15	239.49	98.98	117.67	88.49	79.45	**207.16**	211.91	292.59	130.48	282.65	608.14	83.99	522.81	283.70	62.70
15 - 16	372.05	425.23	48.19	628.40	698.12	302.45	364.86	165.31	565.21	324.71	141.83	65.21	57.21	607.02	448.25	141.27	71.54	76.51	79.91	61.73	129.40	107.70	122.15	87.78	253.77	370.63	50.34	402.62	188.97	49.16
16 - 17	222.36	213.48	36.21	412.90	530.20	163.65	231.26	77.07	342.95	178.84	112.62	52.09	38.96	364.25	328.12	79.73	72.58	55.29	49.84	38.84	63.46	75.22	103.70	70.88	180.66	150.07	35.72	237.88	82.52	32.24
17 - 18	55.31	35.93	35.66	63.40	129.05	37.85	41.85	38.88	75.66	40.61	41.19	40.41	40.98	51.50	43.41	42.71	43.29	43.87	44.44	45.01	46.76	48.48	49.00	47.22	49.45	51.08	48.58	49.61	48.45	48.38
18 - 19	0	0	0	0	0	0	0	0	0	0	0	0	0	0	0	0	0	0	0	0	0	0	0	0	0	0	0	0	0	0
19 - 20	0	0	0	0	0	0	0	0	0	0	0	0	0	0	0	0	0	0	0	0	0	0	0	0	0	0	0	0	0	0
20 - 21	0	0	0	0	0	0	0	0	0	0	0	0	0	0	0	0	0	0	0	0	0	0	0	0	0	0	0	0	0	0
21 - 22	0	0	0	0	0	0	0	0	0	0	0	0	0	0	0	0	0	0	0	0	0	0	0	0	0	0	0	0	0	0
22 - 23	0	0	0	0	0	0	0	0	0	0	0	0	0	0	0	0	0	0	0	0	0	0	0	0	0	0	0	0	0	0
23 - 24	0	0	0	0	0	0	0	0	0	0	0	0	0	0	0	0	0	0	0	0	0	0	0	0	0	0	0	0	0	0
Sum	5763.82	6018.11	906.75	3739.75	8327.71	3518.03	6474.30	4876.93	6416.69	5717.13	1991.02	1924.26	778.37	5209.00	5174.95	3956.55	1559.62	1465.00	1316.84	715.79	2869.40	2886.35	5855.69	1296.18	2836.58	6344.18	1156.74	4850.53	1669.47	661.45

Figure 5. Average daily direct normal irradiation

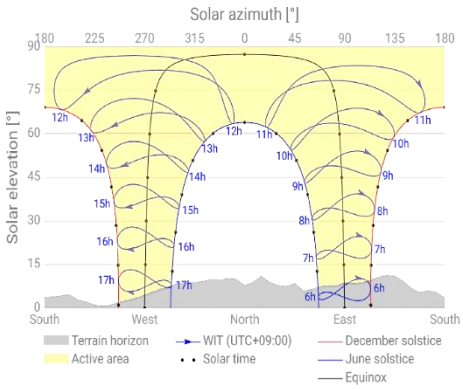

Figure 6. Horizon and path of the sun

The active region of the sun visible above the horizon is highlighted in yellow, while the horizon line is depicted in gray at the base of the diagram. The trajectory of the sun's movement is represented by arrows on the blue curve, facilitating a better understanding of the sun's diurnal movement patterns.

4.2 Panel performance

Table 2 presents the data from the performance measurement results of the MJ2955 transistor-based solar panel, including voltage and electric current strength, along with data on direct normal irradiance (DNI), temperature, and humidity obtained using the Global Solar Atlas and NASA Power Data. The data indicated that the average recorded peak voltage reached 14.96 Volts with a current output of 0.04 mA, observed precisely at 10:00 AM. This peak voltage made it the highest electrical voltage recorded during the measurements, suggesting that the solar panels were functioning under optimal conditions for the absorption and conversion of solar energy.

Additional data points were consistently recorded from 12:00 PM to 02:00 PM. These observations demonstrate that, despite a decrease in sunlight intensity, the solar panels maintained an optimal efficiency level regarding their electric current generation capability [36, 37].

Table 2. Data on voltage and current measurements

Time	T (℃)	RH (-)	P_{in} (W)	V (Volt)	I (mA)
9.00	27.58	0.82	0.083	14.37	0.03
10.00	27.76	0.81	0.047	14.96	0.04
11.00	27.98	0.79	0.029	14.83	0.04
12.00	28.16	0.78	0.035	14.93	0.03
13.00	28.33	0.76	0.048	14.49	0.04
14.00	28.43	0.76	0.047	14.64	0.03
15.00	28.40	0.76	0.036	13.48	0.02

4.2.1 Data analysis

The findings from the descriptive statistical examination (Table 3) suggest that the average temperature stands at 27.83°C. The mean value of relative humidity (RH) stands at 0.78 along with a standard deviation of 0.02, demonstrating notable stability, with recorded lows of 0.76 and highs of 0.82. The input power (W) has a mean of 0.041 with a notably minimal standard deviation of 0.017, signifying consistency, with a range spanning from 0.029 to 0.083. The voltage (V) exhibits an average of 14.73 along with a standard deviation of 0.54, suggesting minor fluctuations within a range of 13.48 to 14.96. Concurrently, the current (A) has the lowest mean, which is 0.03 with the least standard deviation (0.01), reflecting exceptionally high stability with a range of 0.02 to 0.04. This data signifies that the observed system is in a stable and regulated condition.

Table 3. Summary of descriptive statistics of data

Variable	Mean	Median	Std. Dev.	Min	Max
Temperature (°C)	27.83	28.16	0.28	27.58	28.43
Relative Humidity	0.78	0.76	0.02	0.76	0.82
Power Input (W)	0.041	0.047	0.017	0.029	0.083
Voltage (V)	14.73	14.76	0.54	13.48	14.96
Current (A)	0.03	0.04	0.01	0.02	0.04

Table 4. Correlation matrix

	T (℃)	RH (-)	P_{in} (W)	V (Volt)	I (A)
T	1	-0.99	-0.58	-0.36	-0.34
RH	-0.99	1	0.55	0.38	0.3
P_{in}	-0.58	0.55	1	-0.08	-0.06
V	-0.36	0.38	-0.08	1	0.75
I	-0.34	0.3	-0.06	0.75	1

The correlation matrix displayed in Table 4 highlights an extremely robust negative correlation of -0.994 between temperature (T) and relative humidity (RH), indicating that as temperature rises, relative humidity is likely to decrease nearly perfectly. This inverse association is anticipated, as warmer air possesses a greater capacity to retain moisture. There is also a moderate negative correlation of -0.580 between temperature and input power (Pin), implying that elevated temperatures may culminate in reduced power requirements, potentially attributable to diminished efficiency at heightened temperatures. On top of that, temperature manifested slight negative connections of -0.357 with voltage (V) and -0.342 with current (I). Conversely, relative humidity displayed a moderate positive correlation of 0.554 with power input, suggesting that augmented humidity could engender higher power demand. Additionally, there was a moderate positive correlation of 0.379 between relative humidity and voltage. Measured at 0.750, the interplay of voltage and current is considerable, in harmony with Ohm's Law, which suggests that higher voltage usually correlates with higher current.

4.2.2 Panel power and efficiency analysis

The electrical output energy produced by the photovoltaic panels and the overall efficacy of the panels are computed utilizing Eqs. (1) and (2), with the findings succinctly delineated in Table 5. At 09:00 AM, the mean electrical voltage was documented at 14.37 Volts, accompanied by a mean current measurement of 0.03 milliamperes, culminating in an output energy of 0.00043 Watts.

Table 5. Performance of MJ2955 transistor panels

V (Volt)	I (mA)	P_{out} (W)	W (ohm)	DNI (W/m^2)	P_{in} (W)	η_{Panel} (%)
14.37	0.030	0.000431	479.00	475.76	0.083	0.518
14.96	0.040	0.000598	373.92	267.45	0.047	1.278
14.83	0.037	0.000544	404.55	167.75	0.029	1.853
14.93	0.033	0.000498	448.00	202.35	0.035	1.406
14.49	0.043	0.000628	334.46	273.30	0.048	1.313
14.64	0.030	0.000439	487.89	269.86	0.047	0.930
13.48	0.020	0.000270	674.17	207.16	0.036	0.744

At 10:00 AM, an observable rise occurred in the typical

voltage, achieving 14.96 Volts, while the typical current also rose to 0.04 mA, resulting in a power output of 0.00060 watts.

Subsequent to this observation, at 11:00 AM, the mean electrical voltage experienced a slight diminution to 14.83 Volts while sustaining a mean current of 0.04 mA, resulting in a power output of 0.00054 Watts.

Simultaneously, at noon, the typical electrical voltage edged up to 14.93 Volts, paired with a typical current of 0.03 mA, generating a power output of 0.00050 Watts.

The average voltage level recorded at exactly 01:00 PM. dropped significantly, settling at 14.49 Volts, accompanied by an average current measurement of 0.04 milliamperes, resulting in a power output of 0.00063 Watts.

At 02:00 PM, there was a marginal escalation in the mean voltage, which ascended to 14.64 Volts, whereas the mean current diminished marginally to 0.03 milliamperes, culminating in a power output of 0.00044 Watts.

However, when the clock showed 03:00 PM, the average electrical voltage dropped abruptly to 13.48 Volts, with the average electrical current decreasing to 0.02 milliamperes, resulting in the lowest power output of 0.00027 Watts.

In the time span from 09:00 AM to 03:00 PM, this section summarizes the changes in environmental conditions and performance characteristics resulting from the panel system. At 09:00 AM, the average voltage was confirmed to be 14.37 Volts, with an associated average current of 0.03 milliamperes, culminating in a panel power output of 0.00043 Watts and an efficiency rating of 0.518%. By 10:00 AM the primary voltage and resulting power exhibited a progressive increase, with the mean voltage reaching 14.96 Volts and the mean current climbing to 0.04 milliamperes, culminating in a panel power output of 0.000598 Watts and achieving a maximum efficiency of 1.278% (Figure 7).

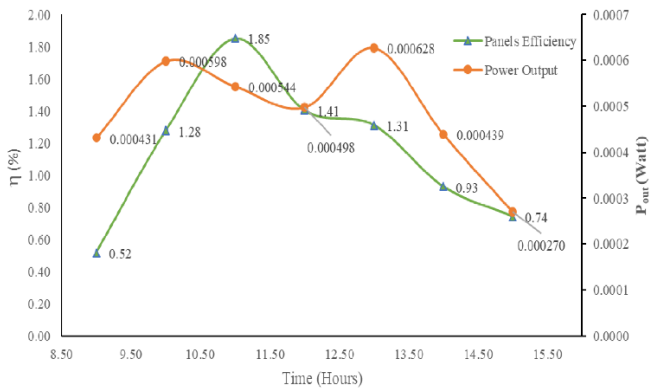

Figure 7. Time to output power and panel efficiency

However, when 01:00 PM was reached, even though the power output increased to 0.000628 Watts, there was a slight decrease in the efficiency of the panels, recorded at 1.313%. At 03:00 PM, both the voltage and the panel input and output power experienced significant declines, dropping to 13.48 Volts and 0.000270 Watts, respectively, recording the lowest efficiency for the panels at 0.744% (Figure 8).

This efficiency is much lower than the output reported by Bow et al. [10] who utilized a total of 96 two-terminal 2N3055 transistors with efficiencies between 3.33% and 18.60%. It is also still below the efficiency of commercial solar panels, which have an efficiency of 19.7% with an output power of 330 Watts from Panasonic's HIT N330 solar panels. Other commercial silicon solar panels typically range from 15% to 20% efficiency, with some advanced multi-junction cells achieving even higher percentages [38]. This difference highlights the treatment and use of materials, as well as the number of transistors used.

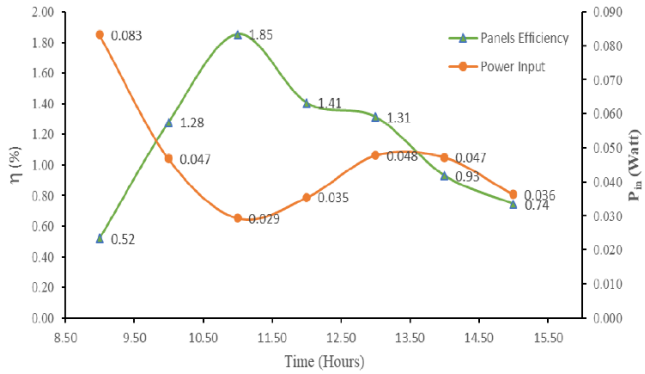

Figure 8. Time to input power and panel efficiency

The relationship between average voltage, average current, panel power, and resistance at various times throughout the day is outlined in Table 5. At 9:00 AM, the measured voltage stood at 14.37 Volts and the current was documented as 0.03 milliamperes, consequently yielding a panel output power of 0.00043 Watts, together with a resistance figure of 479.00 ohms. The increase in voltage and current at 10:00 AM resulted in a panel power output of 0.000598 Watts, accompanied by a lower resistance of 373.92 ohms, indicating that resistance decreased as voltage and current increased. This phenomenon persisted until 11:00 AM and 12:00 PM, during which the resistance progressively augmented, whereas the power output of the panels remained comparatively fluctuating.

At 01:00 PM, voltage and current peaked, resulting in the highest panel power output of 0.000628 Watts, with a corresponding resistance of 334.46 ohms. However, by 02:00 and 03:00 PM, voltage and current began to decrease, resulting in a significant increase in resistance, reaching 674.17 ohms by 03:00 PM, resulting in the lowest panel power output of 0.000270 Watts. These observations demonstrated an inverse relationship between resistance and power generation, where an increase in voltage and current usually leads to a decrease in resistance, thereby improving the efficiency of the solar panel. In contrast, a decrease in voltage and current results in increased resistance, which then reduces power efficiency [39].

4.3 Advantages and limitations of MJ2955 transistor as a solar panel replacement

Based on the thoroughly examined and analyzed data, it is clear that the MJ2955 transistor exhibits several advantages as well as significant limitations that require careful consideration when assessing its feasibility as an alternative to traditional solar panels. The most prominent advantage attributed to this new device is its exceptional variable light absorption efficiency, which shows promise, particularly at 10:00 AM, when its efficiency peaks at an impressive rate of 1.278%. Additionally, the device demonstrates the ability to produce relatively stable power output throughout the day, indicating reliable operational stability. The variation in resistance implies that this device has great potential for improved control and optimization, which could facilitate

achieving peak performance levels, highly beneficial for its application.

Nonetheless, it is imperative to recognize noteworthy limitations that must be contemplated. The considerable and often unpredictable fluctuations in voltage and current indicate a lack of stability in these devices compared to conventional solar panels [40], which generally provide much more consistent and reliable output under a wide range of conditions. Increased resistance levels recorded at certain times of the day—such as 03:00 AM, when a measurement of 674.17 ohms was noted—can severely hamper overall efficiency in power generation. Furthermore, the observed variable efficiency emphasizes a high dependence on fluctuating light intensity, posing challenges in maintaining optimal performance amid changing environmental conditions [41]. The incorporation of advanced tracking systems could potentially alleviate some of these issues by ensuring that the device remains aligned with the sun's trajectory, thereby optimizing sunlight exposure and improving overall energy output.

5. CONCLUSION

The study concluded that the MJ2955 transistor shows significant potential as a replacement for conventional solar panels in simple power generation systems, albeit with some limitations. In terms of efficacy and luminal absorption, the transistor attained a pinnacle efficacy of 1.278% at 10:00 AM, exemplifying its capacity to transmute solar radiation into electrical power, although it persists as less efficacious than conventional photovoltaic modules. The voltage and current attributes illustrate a direct correlation between resistance and output, with diminished resistance yielding elevated voltage and current. Nonetheless, there are significant constraints, such as noticeable voltage and current variations, as seen at 03:00 PM when the resistance increased to 674.17 ohms, along with a low power output of 0.000270 Watts. Despite these issues, using MJ2955 transistors as replacements for solar panels holds promise for low-power applications, especially in remote and isolated environments. Further research is needed to optimize its output power so that the MJ2955 transistor can serve as a viable alternative to certain renewable energy solutions.

ACKNOWLEDGMENT

We thank the Head of the Department of Mechanical Engineering at Cenderawasih University for providing the resources and facilities that enabled us to conduct experiments exploring new approaches to sustainable electrical energy generation.

REFERENCES

[1] Al-Shetwi, A.Q. (2022). Sustainable development of renewable energy integrated power sector: Trends, environmental impacts, and recent challenges. Science of The Total Environment, 822: 153645. https://doi.org/10.1016/j.scitotenv.2022.153645

[2] Sher, F., Curnick, O., Azizan, M.T. (2021). Sustainable conversion of renewable energy sources. Sustainability, 13(5): 2940. https://doi.org/10.3390/su13052940

[3] Shafiullah, M., Ahmed, S.D., Al-Sulaiman, F.A. (2022). Grid integration challenges and solution strategies for solar PV systems: A review. IEEE Access, 10: 52233-52257. https://doi.org/10.1109/ACCESS.2022.3174555

[4] Blaabjerg, F., Yang, Y., Ma, K., Wang, X. (2015). Power electronics - the key technology for renewable energy system integration. In 2015 International Conference on Renewable Energy Research and Applications (ICRERA), Palermo, Italy, pp. 1618-1626. https://doi.org/10.1109/ICRERA.2015.7418680

[5] Morvan, E. (2017). Transistor a enrichissement comportant une heterojonction algan/gan et une grille en diamant dope P. https://patents.google.com/patent/WO2017046077A1/fr.

[6] Jung, J.Y., Kim, S.H., Shinde, S.S., Kim, D.H., Lin, C., Lee, J.H. (2019). (2019). A semiconductor junction photoelectrochemical device without a depletion region. Nanoscale, 11(47): 23013-23020. https://doi.org/10.1039/C9NR08172K

[7] Ekanayake, U.N., Gunapala, S.D., Premaratne, M. (2023). Engineered common environmental effects on multitransistor systems. Physical Review B, 107(7): 075440. https://doi.org/10.1103/PhysRevB.107.075440

[8] Chen, S., Zuo, C., Xu, B., Ding, L. (2021). Monolithic perovskite/silicon tandem solar cells offer an efficiency over 29%. Journal of Semiconductors, 42(12): 120203. https://doi.org/10.1088/1674-4926/42/12/120203

[9] Foster, D.H., Costa, T., Peszynska, M., Schneider, G. (2013). Multiscale modeling of solar cells with interface phenomena. Journal of Coupled Systems and Multiscale Dynamics, 1(2): 179-204. https://doi.org/10.1166/jcsmd.2013.1013

[10] Bow, Y., Dewi, T., Taqwa, A. (2018). Power transistor 2N3055 as a solar cell device. In 2018 International Conference on Electrical Engineering and Computer Science (ICECOS), Pangkal, Indonesia, pp. 327-332. https://doi.org/10.1109/ICECOS.2018.8605203

[11] Kobayashi, E., Watabe, Y., Hao, R., Ravi, T.S. (2015). High efficiency heterojunction solar cells on n-type kerfless mono crystalline silicon wafers by epitaxial growth. Applied Physics Letters, 106(22): 223504. https://doi.org/10.1063/1.4922196

[12] Hu, S.H., Lin, Y.S., Tseng, T.K., Su, S.H., Wu, L.C. (2020). Reducing light reflection by processing the surface of silicon solar cells. Journal of Materials Science: Materials in Electronics, 31: 7616-7622. https://doi.org/10.1007/s10854-020-03253-6

[13] Wang, Y., Wang, Y., Gao, F., Yang, D. (2024). Efficient monolithic perovskite/silicon tandem photovoltaics. Energy & Environmental Materials, 7(3): e12639. https://doi.org/10.1002/eem2.12639

[14] Li, D., Ma, L., Zhang, B., Chen, S. (2022). Facile fabrication of robust and photo-thermal super-hydrophobic coating with efficient ice removal and long-term corrosion protection. Chemical Engineering Journal, 450: 138429. https://doi.org/10.1016/j.cej.2022.138429

[15] Zhang, C., Liu, Z., Zhang, X., Wang, C., Li, M., Yuan, R., Wang, H. (2023). Fabrication of robust superhydrophobic microcapsule-based composite coating with self-healing and anti-scaling properties. Colloids and Surfaces A: Physicochemical and

Engineering Aspects, 671: 131655. https://doi.org/10.1016/j.colsurfa.2023.131655
[16] Polly, S., Bogner, B., Fedorenko, A., Pokharel, N., Ahrenkiel, P., Chowdhury, S., Biswas, D., Hubbard, S. (2023). Growth optimization of quantum-well-enhanced multijunction photovoltaics. Cell Reports Physical Science, 4(6): 101432. https://doi.org/10.1016/j.xcrp.2023.101432
[17] Zou, Y., Qin, C., Liu, H., Zhang, B., Wu, X. (2024). Concentrating photovoltaic systems: A review of temperature effects and components. Journal of Thermal Analysis and Calorimetry, 149(4): 1301–1329. https://doi.org/10.1007/s10973-023-12767-0
[18] Mohamadi, M., Karbasian, M. (2019). Developing an economical model for reliability allocation of an electro-optical system by considering reliability improvement difficulty, criticality, and subsystems dependency. Journal of Industrial Engineering International, 15(2): 379–393. https://doi.org/10.1007/s40092-018-0273-7
[19] Zhou, R., Xu, J., Luo, P., Hu, L., Pan, X., Xu, J., Jiang, Y., Wang, L. (2021). Near-infrared photoactive semiconductor quantum dots for solar cells. Advanced Energy Materials, 11(40): 2101923. https://doi.org/10.1002/aenm.202101923
[20] Guo, S., Hu, Y., Qin, M., Li, J., Wang, Y., Qin, J., Cheng, P. (2022). Toward high-performance organic photovoltaics: the new cooperation of sequential solution-processing and promising non-fullerene acceptors. Materials Horizons, 9(8): 2097-2108. https://doi.org/10.1039/D2MH00376G
[21] Azimi, E., Mehrasa, M., Sharifzadeh, M., Bacha, S., Al-Haddad, K. (2021). Grid integration of an enhanced packed e-cell inverter for renewable energy applications. In IECON 2021 – 47th Annual Conference of the IEEE Industrial Electronics Society, Toronto, ON, Canada, pp. 1-6. https://doi.org/10.1109/IECON48115.2021.9589266
[22] He, Y.L., Qiu, Y., Wang, K., Yuan, F., Wang, W.Q., Li, M.J., Guo, J.Q. (2020). Perspective of concentrating solar power. Energy, 198: 117373. https://doi.org/10.1016/j.energy.2020.117373
[23] Qu, W., Cao, W., Su, Y.C. (2020). Design and implementation of smart manufacturing execution system in solar industry. Journal of Ambient Intelligence and Humanized Computing. https://doi.org/10.1007/s12652-020-02292-5
[24] Westerband, E.I., Hicks, A.L. (2018). Life cycle impact of nanosilver polymer-food storage containers as a case study informed by literature review. Environmental Science: Nano, 5(4): 933-945. https://doi.org/10.1039/C7EN01043E
[25] Kuo, T.C., Kuo, C.Y., Chen, L.W. (2022). Assessing environmental impacts of nanoscale semi-conductor manufacturing from the life cycle assessment perspective. Resources, Conservation and Recycling, 182: 106289. https://doi.org/10.1016/j.resconrec.2022.106289
[26] Smith, M., Bevacqua, A., Tembe, S., Lal, P. (2021). Life cycle analysis (LCA) of residential ground source heat pump systems: A comparative analysis of energy efficiency in New Jersey. Sustainable Energy Technologies and Assessments, 47: 101364. https://doi.org/10.1016/j.seta.2021.101364
[27] Nematchoua, M.K., Sendrahasina, R.M., Malmedy, C., Orosa, J.A., Simo, E., Reiter, S. (2022). Analysis of environmental impacts and costs of a residential building over its entire life cycle to achieve nearly zero energy and low emission objectives. Journal of Cleaner Production, 373: 133834. https://doi.org/10.1016/j.jclepro.2022.133834
[28] Taşer, A., Koyunbaba, B.K., Kazanasmaz, T. (2023). Thermal, daylight, and energy potential of building-integrated photovoltaic (BIPV) systems: A comprehensive review of effects and developments. Solar Energy, 251: 171-196. https://doi.org/10.1016/j.solener.2022.12.039
[29] Pérez-Tomás, A., Lima, A., Billon, Q., Shirley, I., Catalan, G., Lira-Cantú, M. (2018). A solar transistor and photoferroelectric memory. Advanced Functional Materials, 28(17): 1707099. https://doi.org/10.1002/adfm.201707099
[30] Takahashi, A., Moriki, A., Yamada, N., Imai, J., Funabiki, S. (2017). A simple method for measuring solar radiation intensity by image analyses. In 2017 IEEE 44th Photovoltaic Specialist Conference (PVSC), pp. 2906-2911. https://doi.org/10.1109/PVSC.2017.8366101
[31] Coridan, R.H., Nielander, A.C., Francis, S.A., McDowell, M.T., Dix, V., Chatman, S.M., Lewis, N.S. (2015). Methods for comparing the performance of energy-conversion systems for use in solar fuels and solar electricity generation. Energy & Environmental Science, 8(10): 2886-2901. https://doi.org/10.1039/C5EE00777A
[32] Adamo, F., Attivissimo, F., Di Nisio, A., Spadavecchia, M. (2011). Characterization and testing of a tool for photovoltaic panel modeling. IEEE Transactions on Instrumentation and Measurement, 60(5): 1613-1622. https://doi.org/10.1109/TIM.2011.2105051
[33] Jones, R.K. (2021). Improved methodology for typical meteorological year month selection matching annual irradiance. In 2021 IEEE 48th Photovoltaic Specialists Conference (PVSC), Fort Lauderdale, FL, USA, pp. 18-22. https://doi.org/10.1109/PVSC43889.2021.9518562
[34] Leonidov, A.V. (2020). Analytic representation of relation between solar altitude angle and local time for calculating daylight irradiance and illuminance of the earth surface. Light & Engineering, 28(4): 34-38. https://doi.org/10.33383/2019-085
[35] Sari, L.H., Rauzi, E.N., Muslimsyah, Mahmud, M. (2021). Sun-path model as a simple helping tool for architecture students in understanding saving energy building design. IOP Conference Series: Materials Science and Engineering, 1087(1): 012017. https://doi.org/10.1088/1757-899X/1087/1/012017
[36] Mahdi, H.A., Leahy, P.G., Morrison, A.P. (2021). Predicting early EVA degradation in photovoltaic modules from short circuit current measurements. IEEE Journal of Photovoltaics, 11(5): 1188-1196. https://doi.org/10.1109/JPHOTOV.2021.3086455
[37] Farahmand, M.Z., Nazari, M.E., Shamlou, S., Shafie-khah, M. (2021). The simultaneous impacts of seasonal weather and solar conditions on PV panels electrical characteristics. Energies, 14(4): 845. https://doi.org/10.3390/en14040845
[38] Fernández, E.F., García-Loureiro, A.J., Smestad, G.P. (2015). Multijunction concentrator solar cells: analysis and fundamentals. In High Concentrator Photovoltaics,

pp. 9-37. https://doi.org/10.1007/978-3-319-15039-0_2
[39] Myles, A.S., Savadogo, O., Oishi, K. (2019). Concept and simulation study of a novel building integrated photovoltaic thermal (BIPV-T) solar module. Journal of New Materials for Electrochemical Systems, 22(3): 165-172. https://doi.org/10.14447/jnmes.v22i3.a09
[40] Khairunnisa, N., Arifin, Z., Kristiawan, B., Hijriawan, M., Prasetyo, S.D. (2022). Investigation of spirals rectangular and rectangular tubes collector design in photovoltaic solar cell cooling systems. International Journal of Heat and Technology, 40(6): 1359-1365. https://doi.org/10.18280/ijht.400602
[41] Todeschi, V., Marocco, P., Mutani, G., Lanzini, A., Santarelli, M. (2021). Towards energy self-consumption and self-sufficiency in urban energy communities. International Journal of Heat and Technology, 39(1): 1-11. https://doi.org/10.18280/ijht.390101

NOMENCLATURE

A	PNP transistor surface area MJ2955, m^2
DNI	normal direct irradiation, Wh. m^{-2}
I	electric current, A
P_{input}	input power, Watts
P_{output}	ouput power, Watts
V	electrical voltage, Volts
T	temperature, ℃
V	electrical voltage, Volts

Greek symbols

η_{panels}	panel efficiency